https://doi.org/10.1016/j.compstruct.2021.114161

On the FE modelling of RC beams with a fibre-reinforced polymer (FRP)-strengthened web opening

X.F. Nie[1], S.S. Zhang[2, *] and T. Yu[3]

[1] Post-doctoral Fellow, School of Civil and Hydraulic Engineering, Huazhong University of Science and Technology, Wuhan 430074, China.
[2] Professor, School of Civil and Hydraulic Engineering, Huazhong University of Science and Technology, Wuhan 430074, China. (Corresponding author), E-mail address: shishun@hust.edu.cn
[3] Professor, Department of Civil and Environmental Engineering, The Hong Kong Polytechnic University, Hong Kong, China.

Abstract: In order to realize the strong column-weak beam hierarchy in existing reinforced concrete (RC) frames, a novel seismic retrofit technique (i.e., beam opening technique or BO technique) was proposed. The BO technique involves the cutting of a web opening in the RC T-section beam to weaken its flexural capacity, in combination with the installation of a fibre-reinforced polymer (FRP) strengthening system around the opening to offset the loss in shear capacity caused by the opening. While extensive experimental studies have verified the effectiveness of the BO technique, this paper presents a finite element (FE) study on the structural behaviour of RC beams with an FRP-strengthened web opening, for a more comprehensive and in-depth understanding of the performance of such beams. Two constitutive models of concrete were investigated, namely, the concrete damaged plasticity (DP) model and the brittle cracking (BC) model. Through detailed comparisons, it was found that for specimens failing in a flexural mode, the DP model is more appropriate; while for specimens failing in a shear mode, the BC model with the secant modulus of concrete adopted provides better predictions. A simple method for the selection of a proper FE approach is finally proposed.

Keywords: finite element (FE) model; fibre-reinforced polymer (FRP) strengthening; reinforced concrete (RC) beam; web opening; dynamic analysis approach

1. INTRODUCTION

Compared with the storey-sway mechanism under which the plastic hinges first form at the column ends, the beam-sway mechanism under which the plastic hinges first form at the beam ends can result in better seismic performance of reinforced concrete (RC) frames. This is easy to understand as the latter mechanism only affects a limited portion of the structure, while the former mechanism may cause progressive collapse of the entire structure. As an effective way to achieve the beam-sway mechanism of RC frames, the Strong Column-Weak Beam (SCWB) design philosophy has been employed widely in the seismic design codes of RC frames all over the world [e.g. 1-3]. However, investigations on structures failed after major earthquakes revealed that the beam-sway mechanism was seldom realized in the failed RC frames with cast-in-place floor slabs [e.g. 4-6]. As has been analysed in a comprehensive review on the SCWB design philosophy conducted by the authors [7], this situation was mainly caused by the inadequate stipulations/considerations on the SCWB requirement in the design codes (mainly old-version codes). Especially, the enhancement caused by the cast-in-place floor slabs to the flexural capacities of the supporting RC beams was not properly considered in old-version design codes. For example, the previous versions of Chinese seismic design code (i.e., Ref. [8] and previous versions) did not consider the enhancement caused by the cast-in-place floor slabs to both the positive flexural capacity (i.e., flexural capacity of the beam when the floor slab is in compression) and the negative flexural capacity (i.e., flexural capacity of the beam when the floor slab is in tension) of the RC beams. Therefore, it is not unreasonable to believe that a number of existing RC frames violate the SCWB requirement, in which the actual flexural capacities of the RC beams are much larger than their design flexural capacities.

In this context, a novel seismic retrofit method for existing RC frames which violate the SCWB requirement was proposed [9], on the basis of the concept of Beam-end Weakening in combination with fibre-reinforced polymer (FRP) Strengthening (referred to as BWFS method hereafter for simplicity). As one of the proposed techniques to implement the BWFS method, the beam opening (BO) technique includes the cutting of a web opening in the T-section beam to weaken its flexural capacity as well as the installation of a strengthening system around the opening using

FRP to offset the loss in shear capacity caused by the opening [9]. Among the field of composite materials for strengthening existing concrete members [10-18], FRP strengthening has been proved by many researchers to be one of the most effective methods to increase the strength of RC beams. For more details of the BWFS method and the BO technique, the reader can refer to Ref. [9]. To explore the effectiveness of the proposed BO technique, the authors [19, 20] have conducted a series of tests on RC T-section beams with an un-strengthened/FRP-strengthened web opening.

Experimental studies are fundamental for the understanding of the structural behaviour of RC beams with an un-strengthened/FRP-strengthened web opening (as the web openings in an RC beam are generally far apart and there is no interaction between them, beams with more than one web openings are also simply termed as "beams with a web opening" in this paper). They are, however, usually time-consuming and laborious. Finite element (FE) modelling is a powerful and economical alternative to experimental studies [21-23]. Once verified, FE modelling is able to explore more in-depth understanding of the structural behaviour of RC beams [24-26]. Many behavioural aspects (e.g., stiffness, strength and crack propagation) of RC beams with a web opening can be better and/or more effectively examined by using the FE method. Moreover, parametric studies adopting the verified FE model can be used to examine the effect of a wider range of parameters which were not covered in the experimental study on the behaviour of such beams. Therefore, the present study aims to establish an accurate FE model for the RC T-section beams with a web opening tested by the authors [19, 20], in order for more in-depth and comprehensive understanding of the behaviour of such beams.

It is worth noting that the created web openings in existing RC beams can be also used as the passages of utility ducts/pipes. For the RC beams with a web opening created for such purposes, plenty of experimentally-based studies have been conducted to examine their behaviour, including tests on RC rectangular beams with an un-strengthened/FRP-strengthened web opening [e.g. 27-35] and RC T-section beams with an un-strengthened/FRP-strengthened web opening of relatively small size [e.g. 9, 36]. Almost all these tested beams exhibited a shear failure mode caused by the development of diagonal cracks initiated at the web opening corners. Compared with the experimental studies, the relevant numerical studies are much

limited. A literature review on existing numerical studies on RC beams with a web opening has been conducted and presented in previous numerical studies on RC beams with a web opening conducted by the authors [37, 38], and it was found that a proper FE approach for predicting the behaviour of such RC beams had not been well-established. In the previous studies [37, 38], three FE approaches established using ABAQUS [39] have been proposed and assessed by the authors for the modelling of these existing RC beams with an un-strengthened/FRP-strengthened web opening failing in a shear mode. It was found that the brittle cracking (BC) model in which the secant modulus of concrete was adopted provided the closest predictions of the test results. It is worth noting that, however, all the RC T-section beams with an un-strengthened/FRP-strengthened web opening tested by the authors [19, 20] except two beams with an un-strengthened web opening of relatively small size exhibited a flexural failure mode, i.e., plastic hinge formed at each end of the top chord and bottom chord (i.e., the chord above and below the web opening respectively). It has been well acknowledged that the BC model was proposed for applications where the shear and tensile behaviours of cracked concrete dominate the behaviour of the structure [39]. Whether it is also able to give acceptable predictions for test specimens that failed in a flexural mode has not been clarified yet. Therefore, the predictions from the three FE approaches proposed by the authors [37, 38] are compared in this study with the results of the specimens tested by the authors [19, 20], in order to identify the most suitable approach for the FE modelling of RC T-section beams with an FRP-strengthened web opening failing in a flexural mode. Moreover, because the web chord (i.e., the chord in the beam web) was fully wrapped by carbon fibre-reinforced polymer (CFRP) in the specimens tested by the authors [19, 20], the confining effect from the FRP strengthening to the concrete which was not considered in the previously proposed FE approaches [37, 38] is also properly considered in the present study.

2. INTRODUCTION OF THE TESTS

To examine the effectiveness of the proposed BO technique, two batches (Batch-1 and Batch-2) of large-scale RC specimens were tested by the authors [19, 20] under three-point bending, including a total of one rectangular beam and thirteen T-section beams. Details of all test specimens in Batch-1 and Batch-2 are listed in Table 1.

Batch-1 contained eight specimens, including two RC beams without a web opening which served as control beams (one rectangular beam CB-Rec as well as one T-section beam CB-T) and six RC T-section beams with a web opening of large size (with the opening length × opening height being 800 mm × 280 mm or 700 mm × 300 mm). Three beams were tested for each of these two examined large web opening sizes, including one un-strengthened beam tested in negative bending (the beam flange was in tension) (O-800×280-N or O-700×300-N) as well as two FRP-strengthened beams tested in negative bending (F-800×280-N or F-700×300-N) and positive bending (the beam flange was in compression) (F-800×280-P or F-700×300-P), respectively. Batch-2 contained six RC T-section beams with a web opening of small/medium size tested in negative bending. For each of the two examined small web opening sizes (with the opening length × opening height being 700 mm × 200 mm or 600 mm × 220 mm), two specimens were considered, including one un-strengthened beam (O-700×200-N or O-600×220-N) and one FRP-strengthened beam (F-700×200-N or F-600×220-N). For each of the two examined medium web opening sizes (with the opening length × opening height being 700 mm × 260 mm or 600 mm × 280 mm), only one FRP-strengthened beam (F-700×260-N or F-600×280-N) was tested.

Fig. 1 illustrates details of the selected test specimens, including the two control specimens (i.e., CB-Rec and CB-T) and Specimen O-700×300-N as a representative of the tested T-section beams with a web opening. In addition, the layout of the steel reinforcement (including the longitudinal reinforcement and stirrups) is shown in Fig. 1 and listed in Table 1. Fig. 2 shows the adopted CFRP strengthening system for the test specimens with an FRP-strengthened web opening. As shown in Fig. 2, after rounding the corners of the web chord to a radius of 25 mm, one-layer unidirectional CFRP (the thickness is 0.334 mm) was adopted to fully wrap the web chord, in order to enhance the shear capacity and ductility of the web chord; one-layer vertical unidirectional CFRP U-jackets (the thickness and width are respectively 0.334 mm and 200 mm) were applied on the beam web on the two sides of the web opening, in order to mitigate the possible development of diagonal cracks at the corners of the web opening; in addition, to avoid premature debonding of the bonded CFRP U-jackets, CFRP spike anchors were used to anchor the ends of the CFRP U-jackets with the beam flange. The cylindrical compressive strength of concrete for each of the test

specimens is listed in Table 1, and the material properties of the used steel bars and FRP are listed in Table 2.

The test results [19, 20] showed that the two control beams (CB-Rec and CB-T) exhibited a flexural failure mode; the failure of the two RC T-section beams with an un-strengthened web opening of small size (O-700×200-N and O-600×220-N) was controlled by the development of diagonal cracks in the web chord, which is a shear failure mode; in addition, the failure of the two RC T-section beams with an un-strengthened web opening of large size (O-800×280-N and O-700×300-N) as well as all the eight RC T-section beams with an FRP-strengthened web opening was controlled by the formation of four plastic hinges at the two ends of the flange chord and web chord, which is a flexural mode. The reader can refer to Refs. [19] and [20] for more details of the experimental studies.

3. PROPOSED FE APPROACH

3.1. General

The proposed FE approach is a two-dimensional (2-D) FE approach implemented with ABAQUS [39]. The four-node plane stress element CPS4R was adopted to simulate the concrete; the two-node truss element T2D2 was adopted to simulate both the externally bonded FRP and the internal steel reinforcement; and the four-node interfacial element COH2D4 was adopted to simulate the bond behaviour between concrete and both the FRP and the steel reinforcement. COH2D4 is a two-dimensional cohesive element, which can be used to model interfacial debonding between two components, through incorporating the bi-material bond-slip models between these two components [39]. For the rectangular control beam (CB-Rec), the thickness of the plane stress element was set to be the width of the beam; and for the T-section beams, the thickness of the plane stress element for the beam flange was set to be the width of the flange, while that for the beam web was set to be the width of the web. The same method for the simulation of the externally bonded FRP in Ref. [37] was adopted in this study. The two-node truss elements representing the externally bonded FRP were arranged along the fibre orientation of the FRP. For the FRP complete wrap on the web chord (Fig. 2), the upper end of the highest elements of FRP and the lower end of the lowest elements of FRP were fixed onto the top surface and the bottom surface of

the web chord, respectively. For the FRP U-jackets (Fig. 2), the upper end of the highest elements of FRP was fixed onto the upper surface of the web. It should be noted that as the ends of the FRP U-jackets were anchored into the beam flange through CFRP spike anchors (Fig. 2), the lower end of the lowest elements of FRP was also fixed onto the upper surface of the flange. The typical mesh is shown in Fig. 3, in which the red lines stand for FRP sheets. The side length of the elements of concrete was chosen to be 10 mm, based on a convergence study. One FRP/steel element existed between two neighbouring element nodes of concrete, and therefore the length of the FRP/steel elements was also 10 mm. Fig. 3 shows the boundary conditions and applied loads. The vertical and horizontal deformations of the left support were both restrained, and the vertical deformation of the right support was also restrained.

3.2. Modelling of concrete

The concrete damaged plasticity (DP) model and the brittle cracking (BC) model available in ABAQUS/Explicit were both examined in this study. For the DP model, the inelastic behaviour of concrete is simulated using the concepts of isotropic compressive and tensile plasticity in conjunction with isotropic damaged elasticity. Chen et al. [40] have succeeded in adopting the DP model to simulate RC beams without/with FRP-strengthening failing in a flexural mode. The BC model is more applicable for applications where the shear and tensile behaviour of concrete dominates, and it has been successfully adopted by the authors [37, 38] for the simulation of RC beams with an un-strengthened/FRP-strengthening web opening failing in a shear mode. Because of the space limitation, the constitutive equations of concrete as well as the equations of the bi-material bond-slip models which have been detailed in Refs. [37] and [38] are not given in this paper. The reader can refer to Refs. [37] and [38] for more details.

3.2.1. Concrete damaged plasticity (DP) model

In the DP model, the uniaxial compressive stress-strain model developed by Saenz [41] was used to simulate the behaviour of unconfined concrete in compression. For the tested RC T-section beams with an FRP-strengthened web opening, to consider the confining effect from CFRP wrap to the concrete in the web chord, the design-oriented compressive stress-strain curve for the FRP-confined concrete in rectangular columns

developed by Lam and Teng [42] was employed in this study:

$$\sigma_c = \begin{cases} E_c\varepsilon_c - \dfrac{(E_c - E_2)^2}{4f_{co}^{'}}\varepsilon_c^2 & (0 \le \varepsilon_c \le \varepsilon_t) \\ f_{co}^{'} + E_2\varepsilon_c & (\varepsilon_t \le \varepsilon_c \le \varepsilon_{cu}) \end{cases}, \tag{1}$$

$$E_2 = \frac{f_{cc}^{'} - f_{co}^{'}}{\varepsilon_{cu}} \tag{2}$$

$$\varepsilon_t = \frac{2f_{co}^{'}}{E_c - E_2}, \tag{3}$$

$$\frac{f_{cc}^{'}}{f_{co}^{'}} = 1 + k_1 k_{s1}\frac{f_l}{f_{co}^{'}}, \tag{4}$$

$$\frac{\varepsilon_{cu}}{\varepsilon_{co}} = 1.75 + k_2 k_{s2}\frac{f_l}{f_{co}^{'}}\left(\frac{\varepsilon_{h,rup}}{\varepsilon_{co}}\right)^{0.45}, \tag{5}$$

$$f_l = \frac{2\sigma_j t}{D} = \frac{2E_{frp}\varepsilon_j t}{D}, \tag{6}$$

$$\varepsilon_{h,rup} = 0.586\varepsilon_{frp}, \tag{7}$$

$$D = \sqrt{h^2 + b^2}, \tag{8}$$

$$k_{s1} = \left(\frac{b}{h}\right)^{\alpha}\frac{A_e}{A_c}, \tag{9}$$

$$k_{s2} = \left(\frac{b}{h}\right)^{\beta}\frac{A_e}{A_c}, \tag{10}$$

$$\frac{A_e}{A_c} = \frac{1 - ((h/b)(b-2R_c)^2 + (h/b)(h-2R_c)^2)/(3A_g) - \rho_{sc}}{1-\rho_{sc}}, \tag{11}$$

$$A_g = bh - (4-\pi)R_c^2, \tag{12}$$

where ε_c and σ_c are respectively axial strain and axial stress of the confined concrete; E_c and E_2 are respectively elastic modulus of the unconfined concrete and the slope of the straight second portion; $f_{cc}^{'}$ and $f_{co}^{'}$ are respectively compressive strength of the FRP-confined concrete and that of the un-confined concrete; ε_{cu} and ε_t are respectively ultimate axial strain of the confined concrete and the axial strain corresponding to the transition point; k_1 and k_2 are respectively the coefficient of confinement effectiveness (3.3) and the coefficient of strain enhancement (12); k_{s1} and k_{s2} are respectively the shape factor for the strength enhancement and that for the

strain enhancement; f_l and D are respectively confining pressure in and diameter of the equivalent circular column; $\varepsilon_{h,rup}$ and ε_j are respectively the actual hoop rupture strain and nominal hoop rupture strain in the equivalent column; ε_{frp} and σ_j are respectively the ultimate tensile strain of FRP and the corresponding nominal hoop rupture stress; E_{frp} and t are respectively the elastic modulus of FRP in the hoop direction and the total thickness of FRP; b and h are respectively the width and depth of the rectangular column, with $h \geqslant b$; α=2 and β=0.5; $\frac{A_e}{A_c}$ is the effective confinement area ratio; ρ_{sc} is ratio of the cross sectional area of the steel longitudinal reinforcement; R_c is the rounded corner radius; and A_g is gross cross-sectional area of the column with rounded corner.

In addition, in the DP model, the tension-softening curve developed by Hordijk [43] was adopted to simulate the tensile behaviour of cracked concrete, and Rots's model [44] was employed to simulate the shear retention factor.

3.2.2. Brittle cracking (BC) model

In the BC model, the compressive behaviour of concrete is treated as a linear elastic material [39]. For the simulation of the shear and tensile behaviour of cracked concrete, the same shear retention factor model and tension-softening curve employed in the DP model were also adopted in the BC model. It is worth noting that, in the BC model, the concrete in tension is treated as a linear elastic material before reaching its tensile strength. However, actually the tensile stress-strain curve of concrete is nonlinear (as shown in Fig. 4) before reaching its tensile strength, and its modulus decreases constantly with the increase of the tensile stress [45]. Therefore, the initial elastic modulus of concrete ($E_0 = 4730\sqrt{f_c}$ according to ACI-318 [1], where both f_c and E_0 are in *MPa*) and the secant modulus of concrete ($E_{\sec} = \sigma_{to} / \varepsilon_{to}$, where σ_{to} is the peak tensile stress of concrete, and ε_{to} is the corresponding tensile strain, as shown in Fig. 4) were both employed in the BC model for comparison purpose. Following the studies of Ye [45] and Pimanmas [31], the secant modulus of concrete ($E_{\sec}$) was assumed to be one half of the initial elastic modulus of concrete (E_0).

3.3. Simulation of steel bars, FRP and bond behaviour on bi-material interfaces

In this study, the steel bars were assumed to be elastic-perfectly plastic, and the yield stress (as listed in Table 2) was adopted as the strength of the steel bars in the modelling. The externally bonded FRP was simulated as a linear-elastic-brittle material. During loading, debonding between concrete and internal steel bars/external FRP interface may occur, which will reduce the contribution of steel bars/FRP. Therefore, the bond behaviour between concrete and both the steel bars and FRP is important and need to be carefully considered in the FE model. The bond-slip model of CEB-FIP [46] was employed to simulate the shear bond behaviour between concrete and steel bars, while the bond-slip model developed by Lu et al. [47] was employed to simulate the shear bond behaviour between concrete and FRP.

3.4. Dynamic analysis approach

To solve the serious difficulties of numerical convergence caused by the presence of the web opening and the debonding of FRP, the explicit central difference approach which is a dynamic analysis approach available in ABAQUS was adopted in this study. Following the studies of the authors [37, 38], the key factors including the loading time and the damping factor were set as $50T_1$ (T_1 is period of the fundamental vibration mode of the simulated beam) and 1×10^{-5}, respectively. The reader can refer to Refs. [37] and [38] for more details.

3.5. Numerical schemes

In the present study, a total of four numerical schemes were considered: (1) Scheme-1: the behaviour of concrete was simulated using the DP model (referred to as the ***DP model*** hereafter); (2) Scheme-2: the behaviour of concrete was simulated using the DP model, with the confinement effect of FRP strengthening being considered [referred to as the ***DP model (confined)*** hereafter for simplicity]; (3) Scheme-3: the behaviour of concrete was simulated using the BC model, with its secant modulus being adopted (referred to as the ***BC model with SECANT modulus*** hereafter for simplicity); and (4) Scheme-4: the behaviour of concrete was simulated using the BC model, with its initial elastic modulus being adopted (referred to as the ***BC model with INITIAL modulus*** hereafter for simplicity).

For the control specimens, only Scheme-1 was examined, as the DP model has been successfully adopted to simulate RC beams without a web opening in Chen et al.'s study [40]; for the specimens with an un-strengthened web opening, Schemes-1, 3 and 4 were examined; for the specimens with an FRP-strengthened web opening tested in negative bending, Schemes-1 to 4 were examined; and for the specimens tested in positive bending, Schemes-1, 3 and 4 were examined, as the web chord wrapped with FRP is in tension and the confinement effect of FRP wrap to the concrete in the web chord is insignificant.

4. RESULTS AND COMPARISON

4.1. Load-deflection curves

4.1.1. Control beams

Two control beams (without a web opening) were tested, with one being a rectangular beam (CB-Rec) and the other one being a T-section beam (CB-T). Only the DP model was adopted to simulate the two control beams, as they both exhibited a typical flexural failure mode caused by the crushing of the concrete in compression after the yielding of tension steel bars.

The predicted load-deflection curves using the DP model are shown in Fig. 5. The test results are plotted in the same figure for comparison purpose. As can be seen from Fig. 5, for the rectangular control beam (CB-Rec), the predicted load-deflection curve of the specimen using the DP model is very close to the test result (Fig. 5a); for the T-section control specimen (CB-T), the DP model predicts the ultimate load very well, while the predicted cracking load and stiffness of the second segment of the load-deflection curve from FE analysis are much higher than the results obtained from the test (Fig. 5b). Such different performance of the FE model is attributed to the following reasons: (1) in reality, when the applied load is relatively low, a notable shear lag effect exists in the beam flange, which results in non-uniform distributions of the longitudinal tensile stresses in the concrete and reinforcement of the flange across its width direction. The present 2-D model cannot capture such shear lag effects in the flange and thus the predicted cracking load and the second-segment stiffness are higher than the test results; and (2) when the applied load is high enough to make all the longitudinal reinforcement in the flange yield, the tensile stresses in all

these longitudinal steel bars become uniform, and thus the ultimate load of the T-section beam can be well predicted by the present 2-D model.

4.1.2. RC T-section beams with an un-strengthened web opening

A total of four RC T-section beams with an un-strengthened web opening were tested, including O-800×280-N, O-700×300-N, O-700×200-N and O-600×220-N. For Specimens O-800×280-N and O-700×300-N with a web opening of large size, their final failure was dominated by the flexural failure at each end of the flange chord and the web chord; while for Specimens O-700×200-N and O-600×220-N with a web opening of small size, diagonal cracks (at around 30 to 45 degrees with respect to the horizontal line) arose and developed in the span of the web chord and finally dominated the failure of the specimens.

The predicted load-deflection curves using Schemes-1, 3 and 4 are shown in Fig. 6. The test results are shown in the same figure for comparison purpose. As can be seen from Figs. 6a and b, for the RC T-section beams with an un-strengthened web opening of large size (i.e., O-800×280-N and O-700×300-N), the BC model with either SECANT modulus or INITIAL modulus heavily overestimates their strength, while the DP model provides close predictions of the ultimate loads of the specimens. The shape of load-deflection curves predicted using the DP model also matches well with the results obtained from the test, but similar to the situation of the T-section control specimen, the predicted cracking load and the second-segment stiffness are higher than the test results.

As can be seen from Figs. 6c and d, for the specimens with an un-strengthened web opening of small size (i.e., O-700×200-N and O-600×220-N), the DP model heavily underestimates their ultimate loads, the BC model with INITIAL modulus heavily overestimates both their stiffness and strength, while the BC model with SECANT modulus well predicts the ascending portion of the load-deflection curves but still overestimates the ultimate load. The relatively better predictions obtained from the BC model with SECANT modulus for these two specimens is because the two specimens failed in a shear mode, which can be better predicted by the BC model with SECANT modulus as discussed in Refs. [37] and [38].

384 *4.1.3. RC T-section beams with an FRP-strengthened web opening tested in negative*
385 *bending*
386 A total of six RC T-section beams with an FRP-strengthened web opening were tested
387 in negative bending, including F-800×280-N, F-700×300-N, F-700×260-N,
388 F-600×280-N, F-700×200-N and F-600×220-N. The shear cracks at the opening
389 corners were well prevented/restricted, owing to the application of the CFRP wrap
390 and the CFRP U-jackets. The failure of all these specimens was dominated by the
391 flexural failure (formation of plastic hinges) at each end of the flange chord as well as
392 the web chord.
393
394 The predicted load-deflection curves using Schemes-1 to 4 are shown in Fig. 7. The
395 test results are shown in the same figure for comparison purpose. As can be seen from
396 Fig. 7, for all six RC T-section beams with an FRP-strengthened web opening tested
397 in negative bending, both the BC model with SECANT modulus and the BC model
398 with INITIAL modulus heavily overestimate their strength, while the DP model
399 without considering the confinement effect from the FRP strengthening heavily
400 underestimates the ultimate load. With the confinement effect from the FRP
401 strengthening considered, the DP model gives very close predictions of ultimate loads
402 from the tests for all the six beams. The predicted cracking load and second-segment
403 stiffness are again larger than the test results, due to the reason explained earlier.
404
405 *4.1.4. RC T-section beams with an FRP-strengthened web opening tested in positive*
406 *bending*
407 Two RC T-section beams with an FRP-strengthened web opening (i.e., F-800×280-P
408 and F-700×300-P) were tested in positive bending. Similar to the specimens with an
409 FRP-strengthened web opening tested in negative bending, these two specimens also
410 exhibited a flexural failure mode with plastic hinges forming at each end of the flange
411 chord as well as the web chord.
412
413 The obtained load-deflection curves using Schemes-1, 3 and 4 are shown in Fig. 8.
414 The test results are shown in the same figure for comparison purpose. As can be seen
415 from Fig. 8, for both specimens, all three examined schemes overestimate the strength
416 and stiffness. The gap between the prediction and the test can be possibly caused by
417 the following reasons: (1) the shear lag effect existing in the beam flange resulted in

the non-uniform distribution of longitudinal compressive stresses in the beam flange (including the concrete and the reinforcement) across its width, and the current 2-D model with plane stress elements cannot capture such shear leg effects; and (2) the width-to-depth ratio of flange is relatively large (1450/100=14.5). Under compression, therefore, the flange could undergo out-of-plane deformation, which also cannot be reflected by the current 2-D model. The above limitations/simplifications of the present 2-D model can result in overestimation of the ultimate load of the beam. To resolve this problem, a more advanced 3-D FE model needs to be developed in the future.

4.1.5. Comparison of ultimate load

The FE predicted ultimate loads of all beams tested by the authors [19, 20] are compared with test results in Fig. 9 and Table 3. It should be noted that in Fig. 9 and Table 3, for the RC T-section beams with an FRP-strengthened web opening tested in negative bending, the term "DP model" means the DP model with the confinement effect from FRP strengthening being considered. As can be seen from Table 3 and Fig. 9, the DP model provides the best predictions of the ultimate loads of the test specimens, with the average prediction-to-test ratio, standard deviation (STD) and standard deviation (STD) being 0.999, 0.129, and 0.129, respectively. The BC model with SECANT modulus and the BC model with INITIAL modulus respectively give an average prediction-to-test ratio of 1.25 and 1.38, a STD of 0.153 and 0.150, and a CoV of 0.122 and 0.108. Although the latter two models give a smaller value of CoV to the DP model, both models heavily overestimate the ultimate loads. As shown in Fig. 9, there is a much smaller scatter between the test results and the FE predictions from the DP model, which also verifies the better performance of the DP model.

4.2. Failure mode

The predicted crack patterns at failure of all the beams tested by the authors [19, 20] are plotted in Fig. 10, in which the predicted crack patterns of the two beams with an un-strengthened web opening of small size (i.e. O-700×200-N and O-600×220-N) were obtained using the BC model with SECANT modulus and the predicted crack patterns of the other beams were obtained using the DP model. The reason why different models were used for specimens with different failure modes is explained in the next section. The corresponding test crack patterns at failure are also shown in Fig.

10 for comparison purpose. As shown in Fig. 10, for all the beams tested by the authors [19, 20], the predicted crack patterns match well with the test observations.

5. SELECTION OF FE APPROACH

5.1. General

As has been found from the previous studies [37, 38], for RC beams with an un-strengthened/FRP strengthened web opening exhibiting a shear failure mode, the BC model with SECANT modulus gives the closest prediction. From the present study, it is found that for specimens tested by the authors [19, 20] and failed in a shear mode, the BC model with SECANT modulus also gives the closest prediction; differently, for specimens tested by the authors [19, 20] and failed in a flexural mode, the DP model (with the confinement effect from FRP strengthening being considered for the RC beams with an FRP-strengthened web opening) gives the closest prediction, while the BC model with SECANT modulus heavily overestimates the ultimate load. The selection of the proper FE approach is therefore dependent on the particular failure mode of the beam with a web opening, and the following procedure is proposed:

1) Identify the critical chord, which is the web chord in a T-section beam or the chord with a smaller reinforcement ratio between the bottom and top chords in a rectangular beam;
2) Obtain the flexural capacities of the critical chord M_{cs} and M_{ch}, respectively in sagging bending and hogging bending;
3) Obtain the shear capacity of the critical chord V_c; and
4) If V_c is smaller than the value of ($M_{cs}+M_{ch}$) divided by the length of the chord, the beam will fail in shear owing to the development of diagonal cracks in the opening region, and the BC model with SECANT modulus should be adopted; otherwise, the beam will fail in a flexural mode owing to the formation of four plastic hinges at each end of the two chords, and the DP model should be adopted.

The flexural capacity of the critical chord can be easily acquired based on a cross-section analysis, while the shear capacity of the critical chord can be calculated based on certain design equations. It is worth noting that although the Chinese design

codes were used to obtain the shear capacities of un-strengthened chord (using GB-50010 [48]) and strengthen chord (using GB-50608 [49]) in the present study, other relevant design provisions can also be used if the Chinese codes are not available.

5.2. Shear capacity of un-strengthened chord

Without FRP strengthening, the shear capacity of the critical chord (V_c) can be obtained using the following equation [48]:

$$V_c = V_{cc} + V_{cs} = 0.7 f_t b_c h_0 + f_{yv} \frac{A_{sv}}{s_s} h_s, \quad (13)$$

where V_{cc} and V_{cs} are the contributions to the shear capacity of the critical chord from concrete and steel stirrups, respectively; f_{yv} and f_t are the tensile strength of the steel stirrup and concrete, respectively; b_c and h_0 are the width and the effective height of the chord, respectively; A_{sv} is sum of cross-sectional areas of vertical legs of a stirrup at a certain cross-section of the chord; s_s is the distance between two adjacent stirrups; h_s is the height of the stirrup and is assumed to be the actual height of the steel stirrup minus the diameter of the steel stirrup in the present study (i.e., the steel stirrups in the chord are cut by the web opening, and the anchorage length of the steel stirrup is supposed to be the diameter value of the stirrup in this study). It should be noted that the above assumption was adopted to simplify the problem but there have been no exisitng studies which can support this assumption. Its accuracy/validity, therefore, needs furhter investigations in the future.

5.3. Shear capacity of FRP-strengthened chord

If the critical chord is strengthened in shear using FRP, the shear capacity of the chord can be obtained using the following equation [49]:

$$V_c = V_{cc} + V_{cs} + V_{cf}, \quad (14)$$

where V_{cf} is the FRP contribution to the shear capacity of the critical chord and can be calculated as follows.

For FRP complete wraps,

$$V_{cf} = 2\frac{w_f t_f}{(s_f + w_f)}\sigma_{f,vd} h_f (\sin\alpha + \cos\alpha), \quad (15)$$

$$\sigma_{f,vd} = \min\{E_f \varepsilon_{fe,v}, f_{fd}\}, \quad (16)$$

$$\varepsilon_{fe,v} = \frac{8}{\sqrt{\lambda_{Ef}} + 10}\varepsilon_{fd}, \quad (17)$$

$$\lambda_{Ef} = 2\frac{n_f \omega_f t_f}{b(s_f + \omega_f)}\frac{E_f}{f_t}, \quad (18)$$

where w_f and t_f are respectively the width and the thickness of the FRP sheet; s_f is the clear distance between two adjacent FRP sheets; $\sigma_{f,vd}$ is the effective tensile stress of the FRP sheet; h_f is the height of the FRP sheet; α is the angle between the axis of the beam and the orientation of the FRP; f_{fd} and E_f are respectively the tensile strength and the elastic modulus of the FRP sheet; $\varepsilon_{fe,v}$ is the effective strain of the FRP sheet; λ_{Ef} is the characteristic value of shear strengthening; ε_{fd} is the maximum tensile strain of the FRP sheet; and n_f is the layers of the FRP sheet.

For FRP U-jackets or side bonded FRP sheets,

$$V_{cf} = K_f \tau_b w_f \frac{h_f^2}{s_f + w_f}(\sin\alpha + \cos\alpha), \quad (19)$$

$$K_f = \phi\frac{\sin\alpha\sqrt{E_f t_f}}{\sin\alpha\sqrt{E_f t_f} + 0.3 h_f f_t}, \quad (20)$$

$$\tau_b = 1.2\beta_w f_t, \quad (21)$$

$$\beta_w = \sqrt{\frac{2.25 - w_f/(s_f + \omega_f)}{1.25 + w_f/(s_f + \omega_f)}}, \quad (22)$$

where K_f is the coefficient of FRP debonding; τ_b is bond strength between the FRP sheet and concrete; ϕ is the coefficient of FRP strengthening scheme, ϕ=1 for side bonded FRP sheets and ϕ=1.3 for FRP U-jackets.

5.4. Verification

The feasibility of the above method is verified with the specimens collected from the literature [9, 27, 28, 30, 32-34] and specimens tested by the authors [19, 20], as listed

in Table 4. As can be seen from Table 4, for all specimens that can be well predicted by the BC model with SECANT modulus, the flexural capacity of the critical chord is larger than its shear capacity, while for all specimens that can be well predicted by the DP model, the flexural capacity of the critical chord is smaller than its shear capacity. Therefore, the above proposed method for selection of FE approach is proved to be accurate.

6. CONCLUDING REMARKS

The present paper has presented a numerical study on the structural behaviour of RC T-section beams with an un-strengthened/FRP-strengthened web opening. A total of four FE schemes were examined, and on the basis of the FE modelling results, the following conclusions can be drawn:

1) For the RC T-section beams with an un-strengthened web opening which exhibited a flexural failure mode, the DP model provides the best predictions; while for the RC T-section beams with an un-strengthened web opening which exhibited a shear failure mode, the BC model with SECANT modulus gives the best predictions;
2) For the RC T-section beams with an FRP-strengthened web opening which exhibited a flexural failure mode, the DP model with the FRP confinement effect being properly considered provides the best predictions, while the BC model with either SECANT or INITIAL modulus of concrete significantly overestimates the ultimate load;
3) In conjunction with the findings from the previous studies [19, 20], it can be concluded that the selection of the proper FE approach should depend on the possible failure mode of an RC beam with a web opening: the DP model is recommended for beams failing in a flexural mode, while the BC model with SECANT modulus is recommended for beams failing in a shear mode;
4) A simple method, on the basis of the comparison between shear and flexural strength of the critical chord, was proposed in this paper for the proper selection of FE approach. The accuracy of this proposed simple method was validated with the tests collected from the literature as well as tests conducted by the authors; and
5) It should be noted that the outcomes of the present study are also useful for RC

beams with a web opening made for the passages of utility ducts/pipes, although the purpose of creating the web opening is different from that of the present study. In addition, the outcomes of the present study is only applicable to RC beams with a web opening located in a shear span of the beam, while for RC beams with a web opening located in the pure-bending region, further studies need to be conducted in the future.

ACKNOWLEDGEMENTS

The authors are grateful for the financial support received from the Research Grants Council of the Hong Kong Special Administrative Region (Project No.: PolyU 5273/11E) and the National Natural Science Foundation of China (Project No. 51878310 and Project No. 52008183). The work presented in this paper was undertaken under the supervision of Prof. Jin-Guang Teng from The Hong Kong Polytechnic University. The authors are grateful to Prof. Teng for his contributions to this work.

DATA AVAILABILITY

The raw/processed data required to reproduce these findings cannot be shared at this time as the data also forms part of an ongoing study.

REFERENCES

[1] ACI-318 (2019). *Building code requirements for structural concrete and commentary* (*ACI 318-14)*, ACI Committee 318, American Concrete Institute, Farmington Hills, MI.

[2] Eurocode-8 (2004). *Design of structures for earthquake resistance – part 1: general rules, seismic actions and rules for buildings (EN 1998-1: 2004)*, CEN, Brussels.

[3] GB-50011 (2010). *Code for seismic design of buildings*, Architectural & Building Press, Beijing, China (in Chinese).

[4] ATC-40 (1996). *Seismic evaluation and retrofit of concrete buildings*, Applied Technology Council, Redwood City, California.

[5] CABR (2008). *Photo collection of 2008 Wenchuan Earthquake damage to buildings*, Chinese Academy of Building Research, China Architectural & Building Press, Beijing, China (in Chinese).

[6] Chen, H., Xie, Q.C., Dai, B.Y., Zhang, H.Y. and Chen, H.F. (2016). "Seismic damage to structures in the Ms 6.5 Ludian earthquake", *Earthquake Engineering and Engineering Vibration*, 15(1), 173-186.

[7] Nie, X.F., Zhang, S.S., Jiang, T. and Yu, T. (2020). "The strong column-weak beam design philosophy in RC frame structures: a literature review", *Advances in Structural Engineering*, DOI: 10.1177/1369433220933463.

[8] GB-50011 (2008). *Code for seismic design of buildings*, Architectural & Building Press, Beijing, China (in Chinese).

[9] Teng, J.G., Zhang, S.S., Jing, D.H., Nie, X.F. and Chen, G.M. (2013). "Seismic retrofit of RC frames through beam-end weakening in conjunction with FRP strengthening", *Proceedings of the 4th Asia-Pacific Conference on FRP in Structures (APFIS 2013)*, 1-8.

[10] Teng, J.G., Chen, J.F., Smith, S.T. and Lam, L. (2002). *FRP-Strengthened RC Structures*, John Wiley and Sons Ltd, UK, November, 245pp.

[11] Chen, J.F. and Teng, J.G. (2003). "Shear capacity of FRP-strengthened RC beams: FRP debonding", *Construction and Building Materials*, 17(1), 27-41.

[12] Zhang, S.S. and Teng, J.G. (2013). "Interaction forces in RC beams strengthened with near-surface mounted rectangular bars", *Composites Part B: Engineering*, 45(1), 697-709.

[13] Zhang, S.S., Teng, J.G. and Yu, T. (2013). "Bond-slip model for CFRP strips near-surface mounted to concrete", *Engineering Structures*, 56, 945-953.

[14] Teng, J.G., Zhang S.S. and Chen, J.F. (2016). "Strength model for end cover separation failure in RC beams strengthened with near-surface mounted (NSM) FRP strips", *Engineering Structures*, 110, 222-232.

[15] Razaqpur, G., Lamberti, M. and Ascione, F. (2020). "Debonding evolution in nonlinear FRP-retrofitted RC beams with cohesive interface", *Composite Structures*, 236, 111858.

[16] Razaqpur, G., Lamberti, M. and Ascione, F. (2020). "A nonlinear semi-analytical model for predicting debonding of FRP laminates from RC beams subjected to uniform or concentrated load", *Construction and Building Materials*, 233, 117838.

[17] Ascione, F., Lamberti, M., Napoli, A. and Realfonzo, R. (2020). "Experimental

bond behavior of steel reinforced grout systems for strengthening concrete elements", *Construction and Building Materials,* 232, 117105.

[18] Ascione, F., Lamberti, M., Napoli, A., Razaqpur, G. and Realfonzo, R. (2017). "An experimental investigation on the bond behavior of steel reinforced polymers on concrete substrate", *Composite Structures*, 181, 58-72.

[19] Nie, X.F., Zhang, S.S., Teng, J.G. and Chen, G.M. (2018). "Experimental study on RC T-section beams with an FRP-strengthened web opening", *Composite Structures*, 185, 273-285.

[20] Nie, X.F., Zhang, S.S. and Yu, T. (2020). "Behaviour of RC beams with a fibre-reinforced polymer (FRP)-strengthened web opening", *Composite Structures*, 252, 112684.

[21] Abbas, I.A. (2014). "Fractional order GN model on thermoelastic interaction in an infinite fibre-reinforced anisotropic plate containing a circular hole", *Journal of Computational and Theoretical Nanoscience*, 11(2), 380-384.

[22] Abbas, I.A. and Zenkour, A.M. (2014). "Two-temperature generalized thermoelastic interaction in an infinite fiber-reinforced anisotropic plate containing a circular cavity with two relaxation times", *Journal of Computational and Theoretical Nanoscience*, 11(1), 1-7.

[23] Abbas, I.A. (2014). "Three-phase lag model on thermoelastic interaction in an unbounded fiber-reinforced anisotropic medium with a cylindrical cavity", *Journal of Computational and Theoretical Nanoscience*, 11(4), 987-992.

[24] Teng, J.G., Zhang, S.S., Dai, J.G. and Chen, J.F. (2013). "Three-dimensional meso-scale finite element modeling of bonded joints between a near-surface mounted FRP strip and concrete", *Computers and Structures*, 117, 105-117.

[25] Zhang, S.S. and Teng, J.G. (2014). "Finite element analysis of end cover separation in RC beams strengthened in flexure with FRP", *Engineering Structures*, 75, 550-560.

[26] Zhang, S.S. and Teng, J.G. (2016). "End cover separation in RC beams strengthened in flexure with bonded FRP reinforcement: simplified finite element approach", *Materials and Structures*, 49 (6), 2223-2236.

[27] Abdalla, H.A., Torkey, A.M., Haggag, H.A. and Abu-Amira, A.F. (2003). "Design against cracking at openings in reinforced concrete beams strengthened with composite sheets", *Composite Structures*, 60(2), 197-204.

[28] Allam, S.M. (2005). "Strengthening of RC beams with large openings in the shear

661 zone", *Alexandria Engineering Journal*, 44(1), 59-78.
662 [29] Maaddawy, T. and Sherif, S. (2009). "FRP composite for shear strengthening of
663 reinforced concrete deep beams with openings", *Composite Structures*, 89(1),
664 60-69.
665 [30] Madkour, H. (2009). "Non-linear analysis of strengthened RC beams with web
666 openings", *Proceedings of the Institution of Civil Engineers-Structures and*
667 *Buildings*, 162(2), 115-128.
668 [31] Pimanmas, A. (2010). "Strengthening R/C beams with opening by externally
669 installed FRP rods: Behavior and analysis", *Composite Structures*, 92(8),
670 1957-1976.
671 [32] Chin, S.C., Shafiq, N. and Nuruddin, M.F. (2012). "Strengthening of RC beams
672 with large openings in shear by CFRP laminates: experiment and 2D nonlinear
673 finite element analysis", *Research Journal of Applied Sciences Engineering and*
674 *Technology*, 4(9), 1172-1180.
675 [33] Maaddawy, T. and El-Ariss, B. (2012). "Behavior of concrete beams with short
676 shear span and web opening strengthened in shear with CFRP composites",
677 *Journal of Composites for Construction*, 16(1), 47-59.
678 [34] Suresh, J. and Prabhavathy, R.A. (2015). "Behaviour of steel fibre reinforced
679 concrete beams with duct openings strengthened by steel plates", *International*
680 *Journal of Advanced Information in Arts, Science & Management*, 4(4), 40-49.
681 [35] Chin, S.C., Shafiq, N. and Nuruddin, M.F. (2016). "Behaviour of RC beams with
682 CFRP-strengthened openings", *Structural Concrete*, 17(1), 32-43.
683 [36] Mansur, M.A., Tan K.H. and Wei, W. (1999). "Effects of creating an opening in
684 existing beams", *ACI Structural Journal*, 96(6), 899-906.
685 [37] Nie, X.F., Zhang, S.S., Chen, G.M. and Yu, T. (2020). "Strengthening of RC beams
686 with rectangular web openings using externally bonded FRP: Numerical
687 simulation", *Composite Structures*, 148, 112552.
688 [38] Nie, X.F. (2018). *Behavior and modelling of RC beams with an FRP-strengthened*
689 *web opening*, Ph.D Thesis, The Hong Kong Polytechnic University.
690 (http://ira.lib.polyu.edu.hk/handle/10397/80150).
691 [39] ABAQUS (2012). *ABAQUS analysis user's manual (Version 6.12)*, Dassault
692 Systèmes Simulia Corporation, Providence, Rhode Island, USA.
693 [40] Chen, G.M., Teng, J.G. and Chen, J.F. (2011). "Finite element modeling of
694 intermediate crack debonding in FRP-plated RC beams", *Journal of Composites*

for Construction, ASCE, 15(3), 399-353.

[41] Saenz, L.P. (1964). "Discussion of 'Equation for the stress-strain curve of concrete' by P. Desayi and S. Krishan", *ACI Journal*, 61(9), 1229-1235.

[42] Lam, L. and Teng, J.G. (2003). "Design-oriented stress-strain model for FRP-confined concrete in rectangular columns", *Journal of Reinforced Plastics and Composites*, 22(13), 1149-1186.

[43] Hordijk, D.A. (1991). *Local approach to fatigue of concrete*, PhD thesis, Delft University of Technology.

[44] Rots, J.G. (1988). *Computational modeling of concrete fracture*, Ph.D. thesis, Delft University of Technology.

[45] Ye, L.P. (2005). *Concrete Structures* (Second Edition), Tsinghua University Press, Beijing, China (in Chinese).

[46] CEB-FIP (1993). *CEB-FIP Model Code 90*, Thomas Telford, London.

[47] Lu, X.Z., Teng, J.G., Ye, L.P. and Jiang, J.J. (2005). "Bond-slip models for FRP sheets/plates bonded to concrete", *Engineering Structures*, 27(6), 920-937.

[48] GB-50010 (2010). *Code for design of concrete structures*, Architectural & Building Press, Beijing, China (in Chinese).

[49] GB-50608 (2010). *Technical code for infrastructure application of FRP composites*, China Planning Press, Beijing, China (in Chinese).

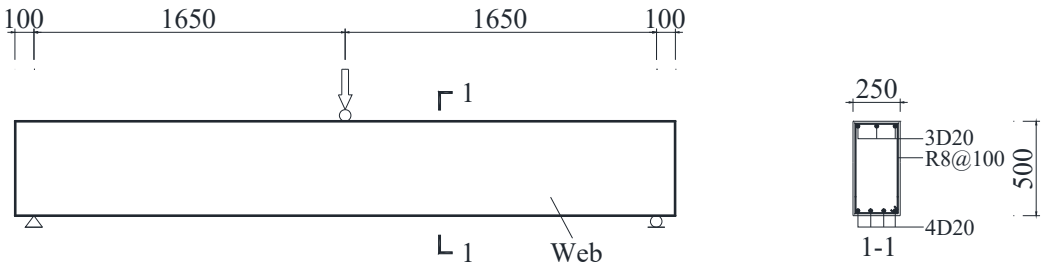

715

716 (a) CB-Rec

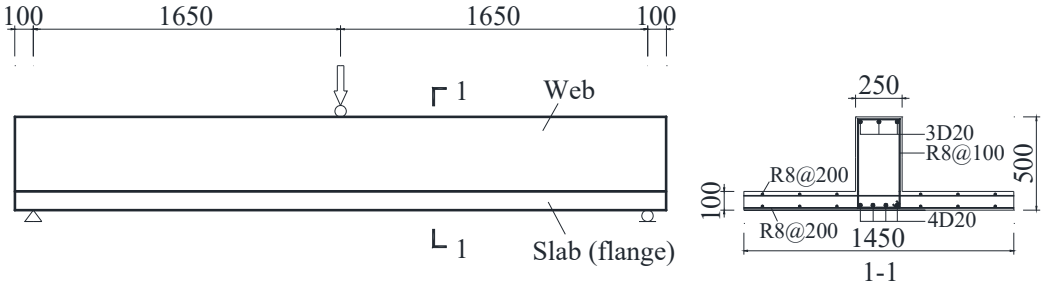

717

718 (b) CB-T

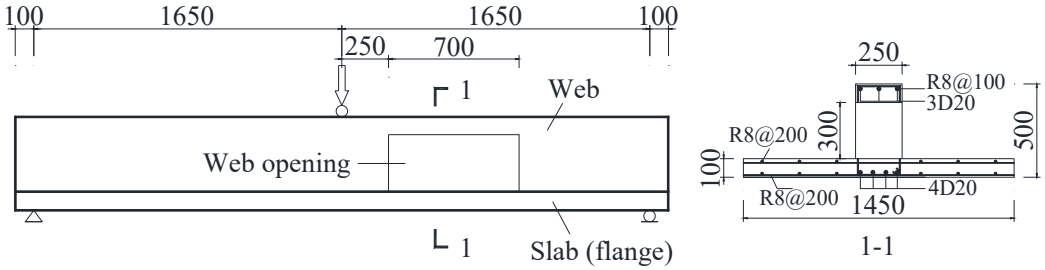

719

720 (c) O-700×300-N

721 Figure 1. Details of test specimen [19, 20] (dimensions in mm)

722

723

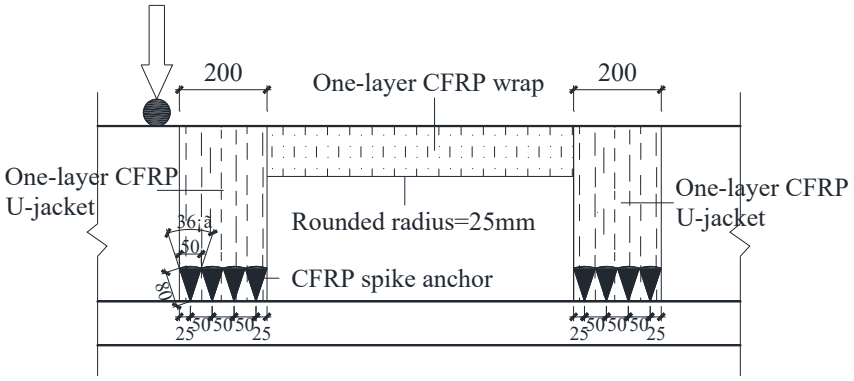

724

725 Figure 2. FRP strengthening system [19, 20] (dimensions in mm)

726

727

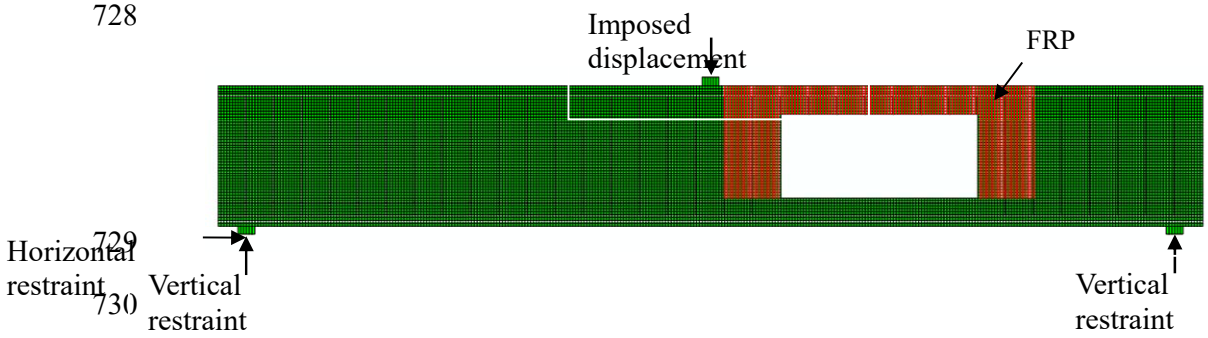

Figure 3. Typical FE mesh

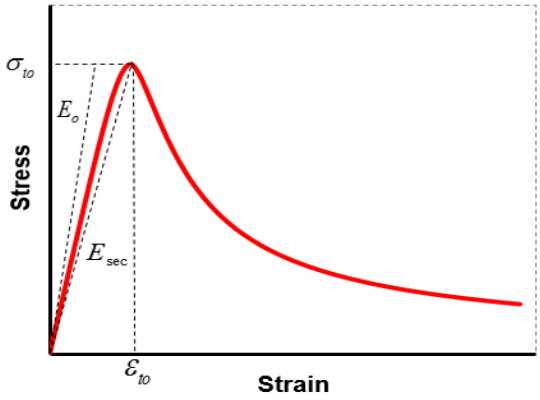

(Note: E_0=initial elastic modulus; E_{sec}=secant modulus)

Figure 4. Tensile stress-strain curve of concrete

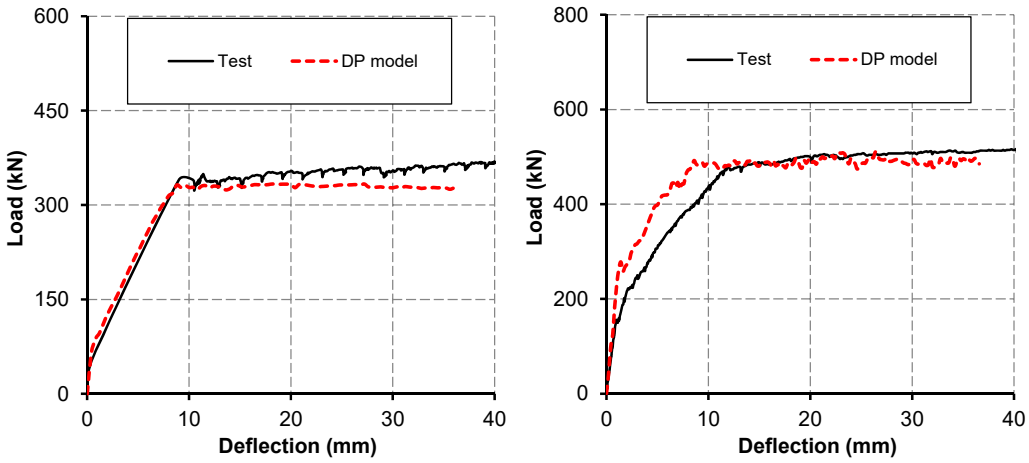

739

740 (a) CB-Rec (b) CB-T

741 Figure 5. Comparison of load-deflection curves between FE predictions and tests:
742 control beams
743

744

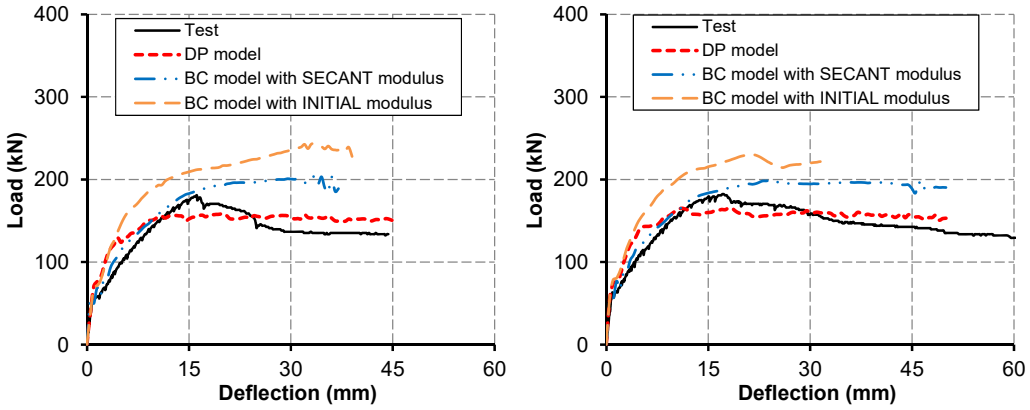

745

746 (a) O-800×280-N (b) O-700×300-N

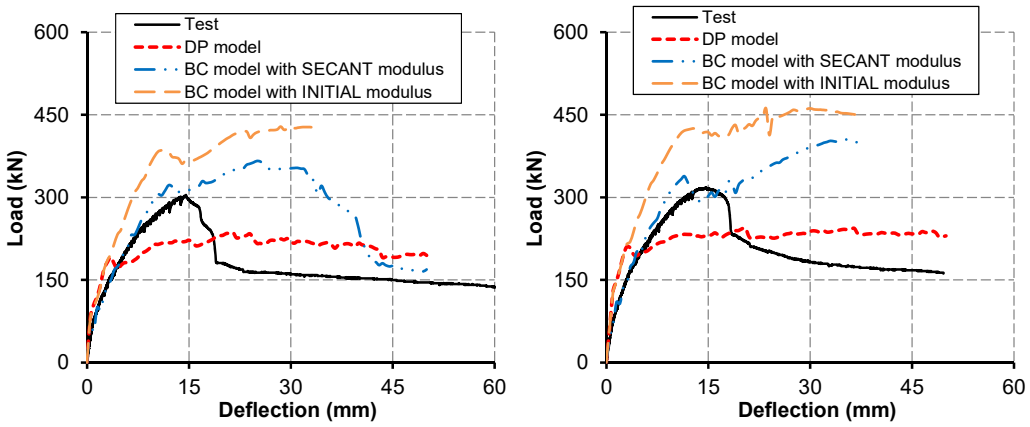

747

748 (c) O-700×200-N (d) O-600×2200-N

749 Figure 6. Comparison of load-deflection curves between FE predictions and tests:
750 T-section beams with an un-strengthened web opening
751

752

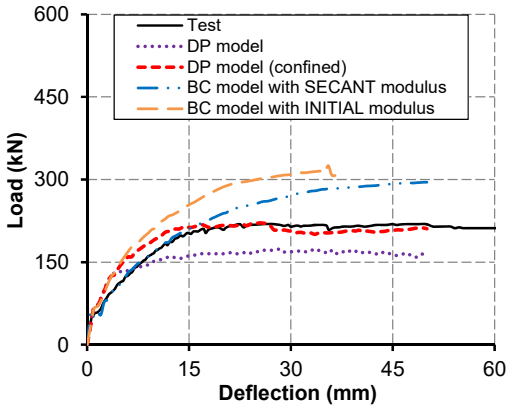

753

754 (a) F-800×280-N

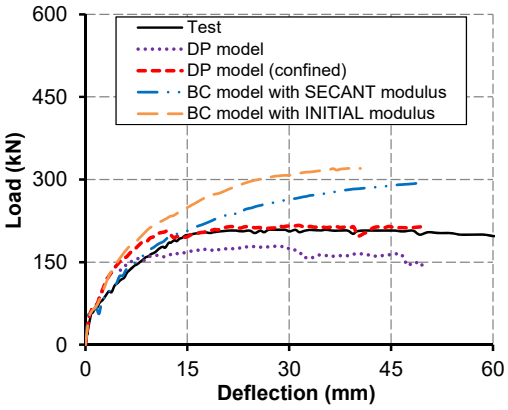

(b) F-700×300-N

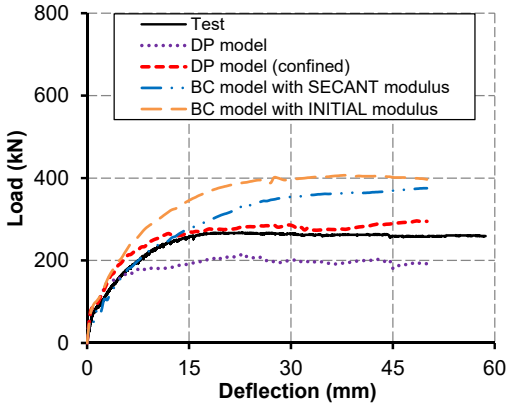

755

756 (c) F-700×260-N

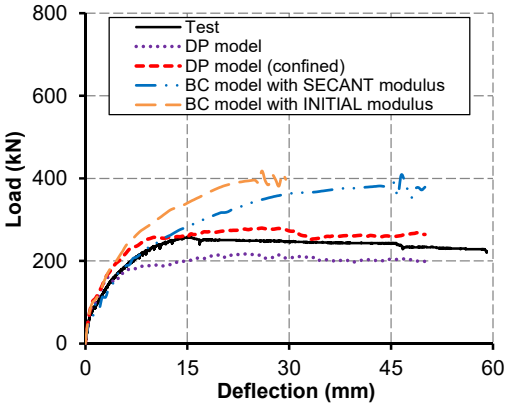

(d) F-600×280-N

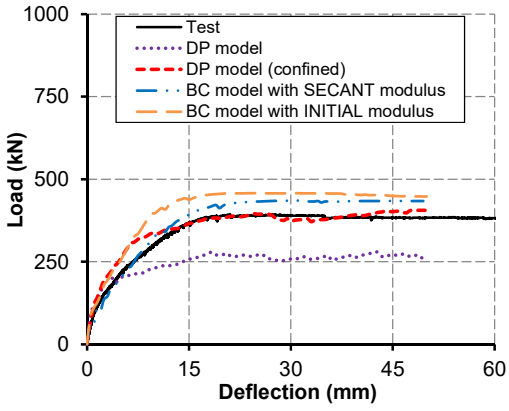

757

758 (e) F-700×200-N

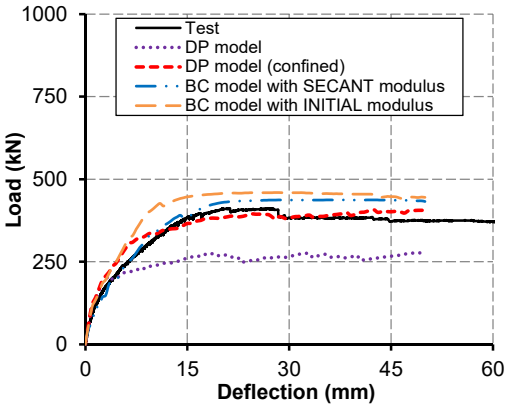

(f) F-600×220-N

759 Figure 7. Comparison of load-deflection curves between FE predictions and tests:
760 T-section beams with an FRP-strengthened web opening tested in negative bending

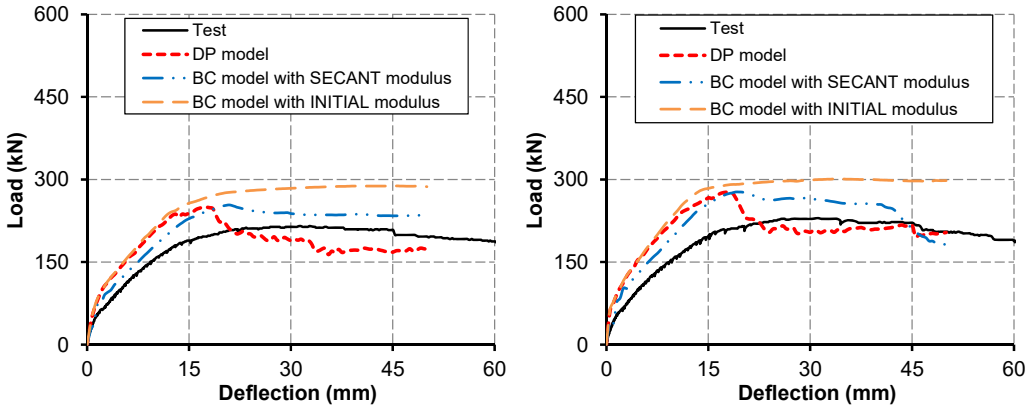

761

762 (a) F-800×280-P (b) F-700×300-P

763 Figure 8. Comparison of load-deflection curves between FE predictions and tests:
764 T-section beams with an FRP-strengthened web opening tested in positive bending
765

766

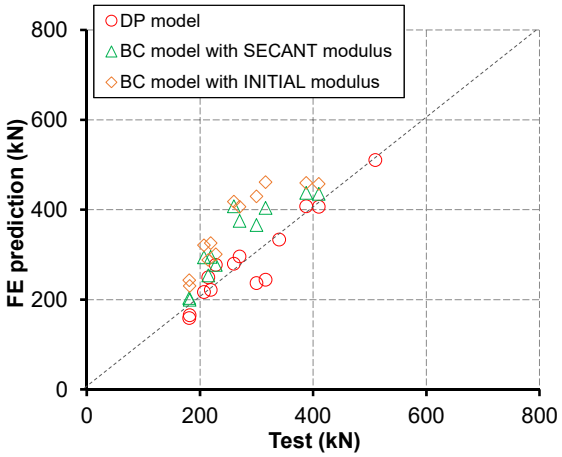

767

768 Figure 9. Comparison of ultimate loads between FE predictions and tests

769

770

771

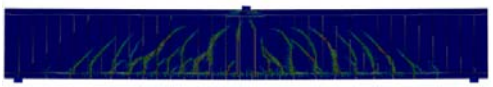

(a) CB-Rec

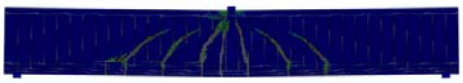

(b) CB-T

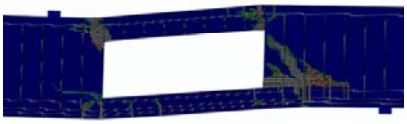

(c) O-800×280-N

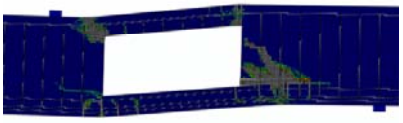

(d) O-700×300-N

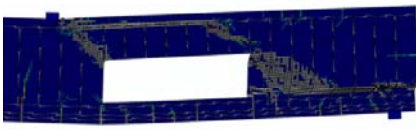

(e) O-700×200-N

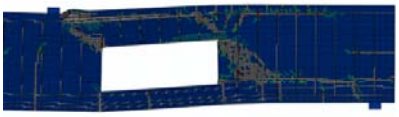

(f) O-600×220-N

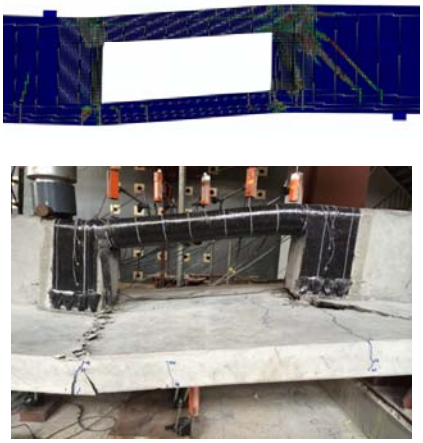

(g) F-800×280-N

(h) F-700×300-N

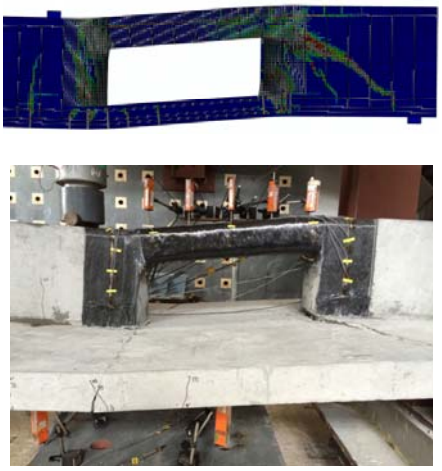

(i) F-700×260-N

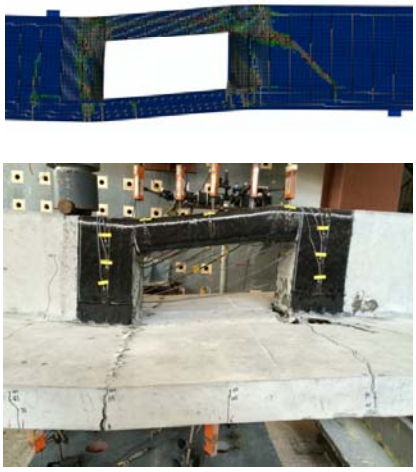

(j) F-600×280-N

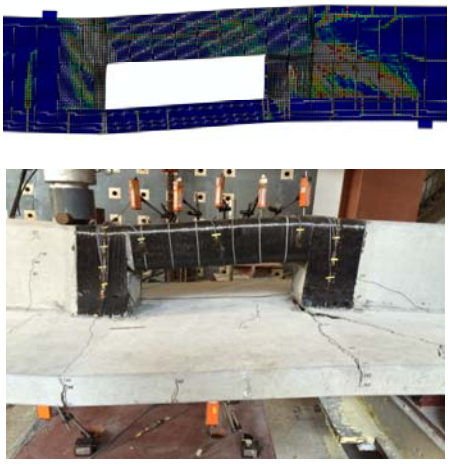

(k) F-700×200-N

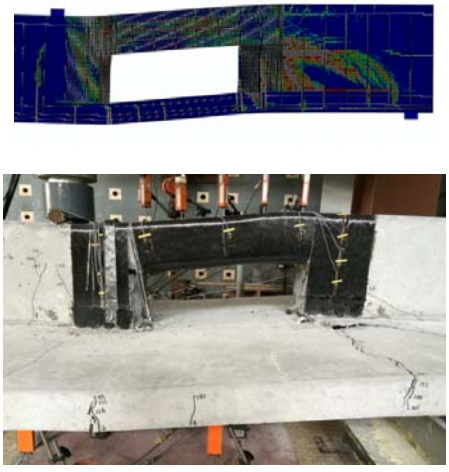

(l) F-600×220-N

(m) F-800×280-P (n) F-700×300-P

Figure 10. Comparison of crack patterns at ultimate state between FE predictions and tests

777 Table 1. Details of the test specimens [19, 20]

Batch	Specimen	Opening size		Web/flange chord height (mm)	FRP strengthening	Bending direction	Cylinder compressive strength of concrete f_c' (MPa)	Steel reinforcement in the web			Steel reinforcement in the flange
		length (mm)	height (mm)					Tension bars	Compression bars	Stirrups	
[1]	CB-Rec	NA	NA	NA	No	Negative bending[(a)]	42.5	4Φ20 (deformed)	3Φ20 (deformed)	Φ8@100 (plain)	-
	CB-T	NA	NA	NA	No	Negative bending	55.2				12Φ8 (plain, placed in two rows)
	O-800×280-N	800	280	120/100	No	Negative bending	42.5				
	F-800×280-N				Yes	Negative bending	41.0				
	F-800×280-P				Yes	Positive bending	44.1				
	O-700×300-N	700	300	100/100	No	Negative bending	42.5				
	F-700×300-N				Yes	Negative bending	41.0				
	F-700×300-P				Yes	Positive bending[(b)]	44.1				
[2]	O-700×200-N	700	200	200/100	No	Negative bending	36.2				
	F-700×200-N				Yes	Negative bending	39.6				
	O-600×220-N	600	220	180/100	No	Negative bending	40.3				
	F-600×220-N				Yes	Negative bending	40.3				
	F-700×260-N	700	260	140/100	Yes	Negative bending	42.0				
	F-600×280-N	600	280	120/100	Yes	Negative bending	42.0				

778 Note: (a) The beam flange was in tension; (b) The beam flange was in compression.
779

Table 2. Material properties of the used steel rebars and FRP [19, 20]

Properties	Batch-1		Batch-2		CFRP sheet
	Steel bars of 20 mm in diameter	Steel bars of 8 mm in diameter	Steel bars of 20 mm in diameter	Steel bars of 8 mm in diameter	
Yield stress (MPa)	475	307	434	349	-
Ultimate stress (MPa)	625	447	559	526	2820
Elastic modulus (GPa)	203	203	203	203	227

Table 3. Test and predicted ultimate loads

Specimen	Test result (kN)	DP model (kN)		BC model with SECANT modulus (kN)		BC model with INITIAL modulus (kN)	
		Prediction	Prediction / test	Prediction	Prediction / test	Prediction	Prediction / test
CB-Rec	340	333.5	0.981	-	-	-	-
CB-T	510	510.5	1.00	-	-	-	-
O-800×280-N	181	158.9	0.878	203.4	1.12	243.0	1.34
O-700×300-N	182	165.2	0.91	199.5	1.10	230.1	1.26
O-700×200-N	300	236.5	0.788	366.1	1.22	429.6	1.43
O-600×220-N	316	243.8	0.772	404.0	1.28	461.6	1.46
F-800×280-N	219	221.5	1.01	295.1	1.35	325.6	1.49
F-700×300-N	207	216.8	1.05	294.0	1.42	320.8	1.55
F-700×260-N	270	296.0	1.10	375.1	1.39	406.7	1.51
F-600×280-N	260	279.7	1.08	407.8	1.57	417.8	1.61
F-700×200-N	410	406.4	0.991	435.5	1.06	457.6	1.12
F-600×220-N	388	407.4	1.05	437.5	1.13	459.6	1.18
F-800×280-P	215	249.6	1.16	253.8	1.18	288.2	1.34
F-700×300-p	228	277.1	1.22	277.5	1.22	300.7	1.32
Average =			0.999		1.25		1.38
STD =			0.129		0.153		0.150
CoV =			0.129		0.122		0.108

Table 4. Comparison of the shear capacity and flexural capacity of the critical chord

Source	Specimen		Shear capacity (kN)		Flexural capacity (kN.m)				$(M_{cs}+M_{cs})/l^{(c)}$ (kN)		Mode of failure	
	Un-strengthened (US)	FRP-strengthened (FS)	US	FS	$M_{cs}^{(a)}$		$M_{ch}^{(b)}$		US	FS	US	FS
					US	FS	US	FS				
Nie et al. [19, 20]	O-700×300-N	F-700×300-N	34.9	95.2	7.0	7.0	14.7	14.7	31.0	31.0	Flexure	Flexure
	O-800×280-N	F-800×280-N	41.1	113.5	7.0	7.0	24.9	24.9	39.8	39.8	Flexure	Flexure
		F-600×280-N	44.1	116.4	6.9	6.9	24.6	24.6	52.6	52.6		Flexure
		F-700×260-N	51.1	135.4	6.9	6.9	32.9	32.9	56.9	56.9		Flexure
	O-600×220-N	F-600×220-N	64.8	172.6	6.6	6.6	48.9	48.9	92.6	92.6	Shear	Flexure
	O-700×200-N	F-700×200-N	71.7	191.4	6.5	6.5	57.0	57.0	90.7	90.7	Shear	Flexure
Teng et al. [9]	O-500×150		93.1		5.6		82.9		177.1		Shear	
		FRP-500×220	66.7	168.0	5.6	37.6	51.1	52.1	113.5	179.4		Shear
Maaddawy and Ariss [33]	CN-500×120	S1-500×120	2.1	22.0.	0.3	7.1	9.0	9.0	18.5	32.2	Shear	Shear
		S2-500×120		23.1								
	CN-500×160	S1-500×160	2.1	16.4	0.3	4.8	6.4	6.4	13.5	22.4	Shear	Shear
		S2-500×160		17.0								
Abdalla et al. [27]	UO8	RO2	11.4	11.4	1.3	>1.3[(d)]	2.3	>2.3	18.3	>18.3	Shear	Shear
	UO9	RO3	11.6	11.6	1.4	>1.4	2.4	>2.4	12.5	>12.5	Shear	Shear
Madkour [30]	E2		4.5		1.0		4.2		8.7		Shear	
	E3		4.5		1.0		3.5		7.4		Shear	
	E4		4.5		1.0		2.6		6.0		Shear	
	E5		4.5		1.0		1.7		4.6		Shear	
Allam [28]	B2	B8	9.7	9.7	1.5	>1.5	7.3	>7.3	19.5	>19.5	Shear	Shear
Suresh and Prabhavathy [34]	NS250		6.24		0.5		2.9		13.5		Shear	
	NS300		6.24		0.5		2.9		11.3		Shear	
Chin et al. [32]	B3	B5	5.1	5.1	0.7	>0.7	1.0	>1.0	8.0	>8.0	Shear	Shear

Note:
(a) The flexural capacity of the chord in sagging bending;
(b) The flexural capacity of the chord in hogging bending;
(c) The length of the chord;

(d) The flexural capacity of the chord after FRP-strengthening doesn't need to be further calculated because the shear capacity of the chord after FRP strengthening is still smaller than the flexural capacity of the un-strengthened chord.